Electron induced nanoscale engineering of rutile TiO2 surfaces

Article (Published Version)

Nanotechnology

PAPER • **OPEN ACCESS**

Electron induced nanoscale engineering of rutile TiO_2 surfaces

To cite this article: David S Humphrey *et al* 2019 *Nanotechnology* **30** 025303

OPEN ACCESS
IOP Publishing
Nanotechnology

Nanotechnology **30** (2019) 025303 (10pp)
https://doi.org/10.1088/1361-6528/aae95b

Electron induced nanoscale engineering of rutile TiO_2 surfaces

David S Humphrey, Chi L Pang[1], Qiao Chen[2] and Geoff Thornton

London Centre for Nanotechnology and Chemistry Department, University College London, 17–19 Gordon Street, London, WC1H 0AJ, United Kingdom

E-mail: g.thornton@ucl.ac.uk

Received 19 June 2018, revised 3 October 2018
Accepted for publication 18 October 2018
Published 9 November 2018

Abstract

Electron stimulated modifications of the rutile TiO_2(110) surface have been investigated using scanning tunnelling microscopy tip pulses and electron beam irradiation. Tip pulses on the 'as-prepared' surface induce local surface reconstruction and removal of surface hydroxyls in a region around the reconstruction. A defocused beam from an electron gun as well as tip pulses have been used to generate a number of oxygen deficient surfaces. All tip pulse features display an oval profile, which can be attributed to the anisotropic conductivity of the TiO_2(110) surface. A novel oxygen deficient phase with well-ordered defective 'nano-cracks' has been identified, which can be produced by either electron beam irradiation or low flash anneal temperatures (~570 K). Annealing such surfaces to moderate temperatures (~850 K) leads to mixed 1×1 and 1×2 surfaces, until now only achievable by annealing in oxygen or ageing by repeated sputter/anneal cycles. Heating to normal preparation temperatures (1000 K) reforms the clean, well-ordered 1×1 surface termination. Our results demonstrate the potential of electron induced processes to modify the oxygen composition and structure of the TiO_2(110) surface in a controllable and reversible way for selective surface patterning and surface reactivity modification.

Keywords: TiO_2, STM, reconstruction, electron beam, tip pulse, surface structure, point defects

(Some figures may appear in colour only in the online journal)

Introduction

The wide-scale implementation of nanotechnology relies on the development of highly controllable and reproducible procedures to fabricate nanoscale objects. As part of this activity, patterning dielectric oxides on the nanoscale with electron beams has been demonstrated [1–3] along with its use to fabricate nanowires [4]. Rutile TiO_2(110) is a model system for such work because the surface physics and chemistry have been widely studied in connection with its multiple applications [5]. Moreover, previous work has shown that TiO_2(110) is a promising candidate for selective functionalisation of surface defects, such as oxygen vacancies (O_{vac}) and step edges [6, 7]. In this work we show that these features can be synthesised and modified using electron induced processes.

Here we employ scanning tunnelling microscopy (STM) as a manipulation tool as well as an atomic scale imaging device. STM tip manipulation has previously been demonstrated to induce local structural alterations and reconstructions, as well as removal of adsorbates [8–11]. For example, removal of hydrogen from a H-passivated Si surface can be used to selectively create Si dangling bonds; these are then reacted with phosphine gas to dope the near surface in a highly controlled way for surface device fabrication [3, 10]. STM-induced modification of structure as well as adsorbate

[1] Surface Science Research Centre and Department of Chemistry, Liverpool University, Liverpool L69 3BX, United Kingdom.
[2] Department of Chemistry, University of Sussex, Falmer, Brighton, BN1 9QJ, United Kingdom.

removal have also been demonstrated for TiO_2(110) [1, 12–16]. This includes the use of high current scans to remove reconstructed 1 × 2 areas to reveal the underlying 1 × 1 periodicity [12], the use of high bias scans to generate structures grown on the 1 × 1 surface [13], and the use of tip pulses to modify the morphology of the 1 × 2 reconstructed surface [14]. The removal of formate and hydrogen has also been demonstrated [15–17]. STM tip pulses have also been used to create areas of the 1 × 2 phase with a width of about 8 nm [1].

As noted above, electron beams delivered from a filament have long been used to modify surfaces, for instance by electron stimulated desorption of oxygen to form O_{vac} in a metal oxide [2, 3, 17, 18]. Previously, we have used this method to enhance the O_{vac} concentration on TiO_2(110) as well as to form (1 × *n*) reconstructions [1, 19].

In this study we combine the use of electron beams from an STM tip and an electron gun to modify TiO_2(110). Metastable phases were created by 3 keV electron bombardment. These surfaces were subjected to electrical pulses from the STM tip, which created areas of the 1 × 2 reconstructed surface up to ~160 × 125 nm^2 in size.

Experimental details

The measurements reported here were recorded using an *Omicron* ultrahigh vacuum (UHV) variable temperature scanning tunnelling microscope (VTSTM), with a base pressure of 1 × 10^{-10} mbar. All STM images were recorded at room temperature using electrochemically-etched tungsten tips. Tips were conditioned by 10 V scans and tip pulses.

Single crystal rutile TiO_2(110)1 × 1 surfaces (*Pi-Kem*) were prepared by cycles of argon ion sputtering at 1 keV and annealing to 1000 K in UHV. The 1 × 2 surface reconstruction forms with extended annealing to 1100–1200 K [12, 20–23]. Sample order and cleanliness were confirmed with low energy electron diffraction (LEED) and Auger electron spectroscopy (AES).

Electron beam (e-beam) irradiation was performed using an electron gun (*Thermo-Electron LEG* 62) defocussed to provide a spot size of 3 mm on the sample. The source was thoroughly degassed prior to e-beam irradiation experiments, and no pressure rise was detected during electron beam exposures. The beam size and position was monitored using a phosphor-coated sample plate.

Electrical tip pulses were performed in the following manner: (1) the bias voltage and tunnelling current are selected; (2) the raster scanning is paused and the tip moved to the chosen lateral position for the pulse; (3) the feedback loop is switched off and the bias voltage is changed to the selected pulse voltage and held for a chosen time period, after which the bias voltage is returned to the previous set point and (4) the raster scan is re-initiated for imaging. STM imaging and pulse conditions are reported with imaging sample bias voltage V_{im}, imaging current setpoint I_{im}, sample pulse voltage V_p, and pulse duration t_p. All imaging and pulses were performed using positive sample bias.

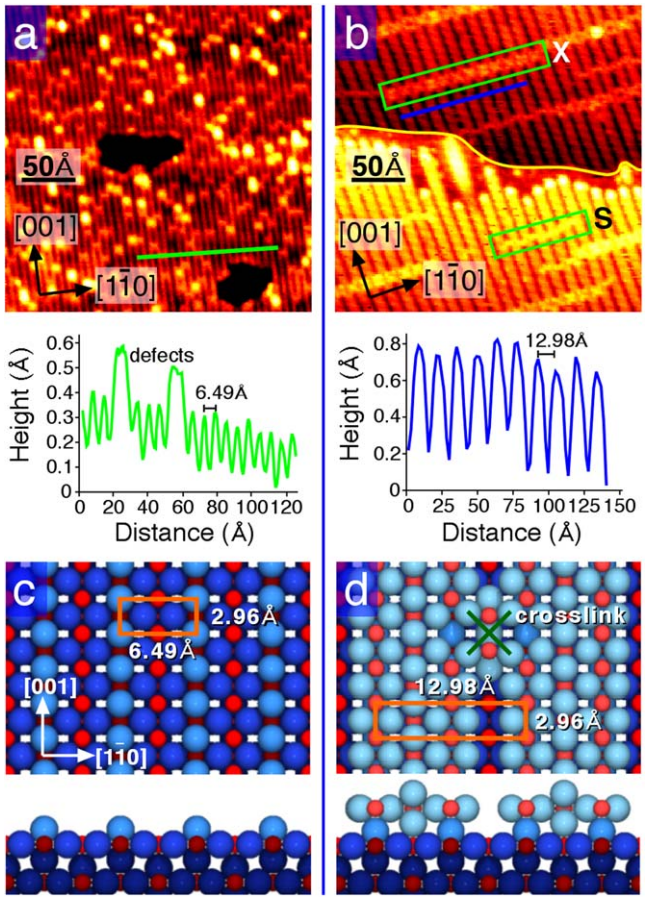

Figure 1. (a) 27 × 27 nm^2 STM image recorded from as-prepared TiO_2(110)1 × 1 (1.5 V, 0.3 nA). (b) 27 × 27 nm^2 STM image of TiO_2(110)1 × 2 with crosslinks (1.5 V, 0.75 nA). Single links (S) as well as crosslinks (X) are indicated (green boxes). The yellow line indicates a 1 × 1 terminated region which is bound by a step edge. Line profiles measured from the position of the green and blue lines show the corrugation and periodicity of the reconstructions. (c) and (d) Ball models show the top and side view, looking along the [001] direction. Blue and red balls correspond to O and Ti atoms respectively, with lighter colours indicating atoms protruding further from the surface. The surface unit cell of each reconstruction is highlighted (orange boxes). The 1 × 2 crosslinked surface model is that proposed in [20].

We note that the energy reported for electrical tip pulses is relative to the Fermi level, whereas for the e-beam irradiation the energy reported is relative to the vacuum level of the e-gun filament.

Results and discussion

As-prepared surfaces

Figure 1 shows STM images of TiO_2(110)−1 × 1 and the 1 × 2 surface reconstruction as well as corresponding structural models [5, 6, 23–25]. The image of the 1 × 1 surface is shown in figure 1(a), with the corresponding model in figure 1(c). It is characterised by alternating bright 5-fold coordinated Ti atoms (Ti_{5f}) and dark bridging oxygen (O_{br})

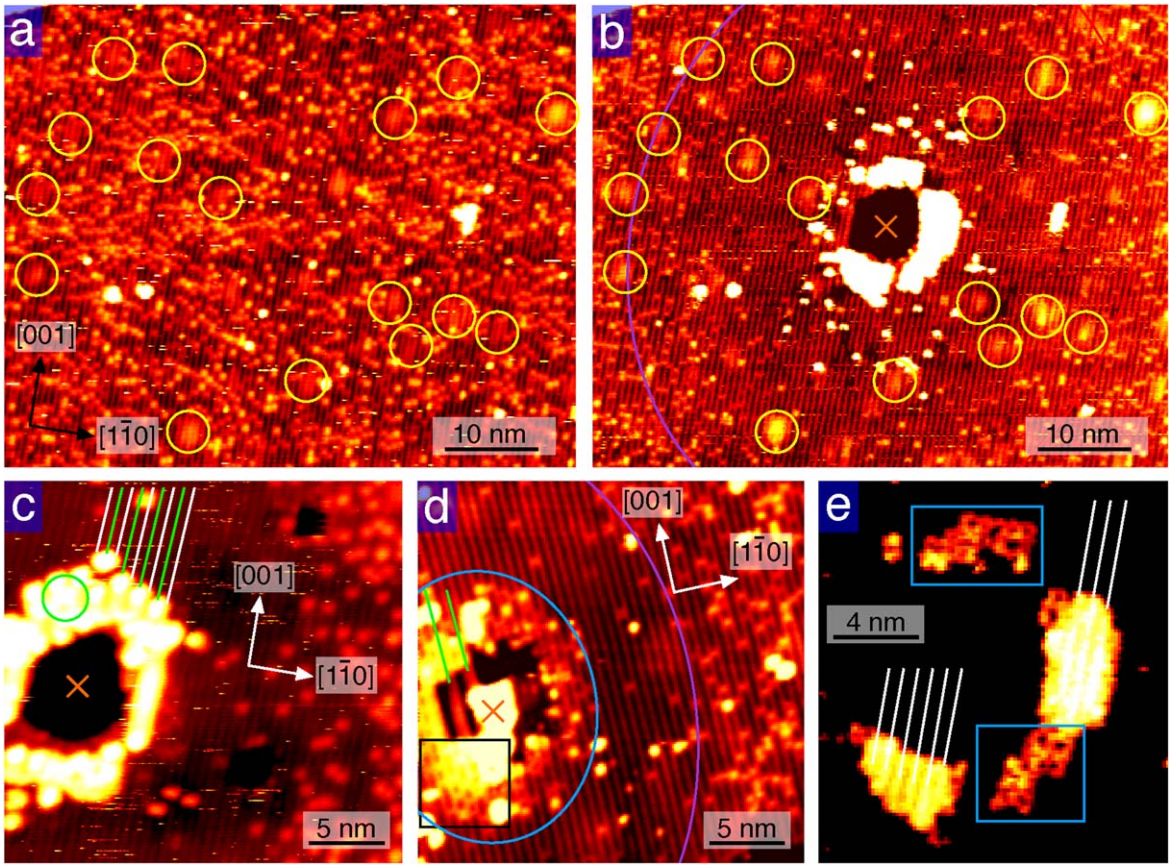

Figure 2. STM images recorded from TiO_2(110)1 × 1 before and after tip pulses. (a) 60 × 48 nm^2 STM image pre and (b) post 10 V pulse (V_{im} = 1.4 V, I_{im} = 0.02 nA, V_p = 10 V, t_p = 1 ms). OH_{br}, O_{vac} and subsurface impurities [26] (yellow circles) are present. The surface around the pulse appears 'healed' with most OH_{br} defects removed (purple line boundary). Subsurface impurities are unchanged in location or appearance. (c) 27 × 25 nm^2 STM image following another 10 V tip pulse in a different area (V_{im} = 1.3 V, I_{im} = 0.02 nA, V_p = 10 V, t_p = 1 ms). The 1 × 1 surface rows are clearly visible. The pulse induced reconstruction consists of 1 × 2 rows terminating in bright features (1 × 2 periodicity highlighted with green lines) and with crosslinks (green circle). (d) 25 × 24 nm^2 STM image following a third 10 V tip pulse in a different area (V_{im} = 1.5 V, I_{im} = 0.5 nA, V_p = 10 V, t_p = 1 ms). The pulse induced reconstruction consists of 1 × 2 rows (green lines), a high concentration of O_{vac} defects (blue line boundary) including elements of a c(4 × 2) reconstruction (black box). The region between the purple and blue lines is 'healed' by removal of OH_{br} defects. (e) 16 × 17 nm^2 high contrast zoom of the pulse induced reconstruction of (b). Added 1 × 1 terraces (white lines indicate the 1 × 1 periodicity) and rosette structures (blue boxes). Orange crosses identify positions of tip pulses.

rows, with bright O_{vac} and bridging hydroxyls (OH_{br}) on O_{br} rows (OH_{br} are brighter). The image of the 1 × 2 surface and its model is shown in figures 1(b) and (d), respectively. 1 × 2 reconstructed terraces are added material on the 1 × 1 termination [23, 25], and as a result are separated by 1 × 1 terminated steps (see figure 1(b)). Surface steps on the 1 × 1 and 1 × 2 surfaces are aligned in the [001], [1$\bar{1}$1] and [$\bar{1}$11] directions, the detailed atomic structures of these steps being well characterised [6]. The STM features associated with the 1 × 1 and 1 × 2 terminations as well as steps form the key structural motifs that are found on the modified surfaces.

Surface tip pulses of the 1 × 1 termination

Figure 2(a) shows the surface before the tip pulse. This serves to identify the presence of subsurface impurites in the image [26]. Figure 2(b) shows the same area after a 10 V tip pulse, with the subsurface impurities unchanged. There are several features to note. One is that *H* atoms on the OH_{br} have been removed from the region around the pulse. Furthermore, after checking the effect of pulses applied from numerous STM tips using several different pulse parameters above 5 V, we conclude that the area affected is always oval in shape with the elongation in the [001] direction. This corresponds to the direction of highest electrical conductivity [27].

A number of reconstructions are observed in the immediate pulse centres. A few selected pulse induced features are shown in figure 2. We have observed a range of additional structures with sizes of ∼10–16 nm. These include high local concentrations of O_{vacs}, 1 × 2 areas with crosslinking, rosette-like structures (seen previously for reoxidation of reduced surfaces [28]), and added 1 × 1 terraces. These reconstructions and added material are all well known phases of TiO_2 reconstructions, each with differing oxygen composition. This suggests that material is removed from and redeposited onto the surface during a pulse, as suggested in earlier work [1].

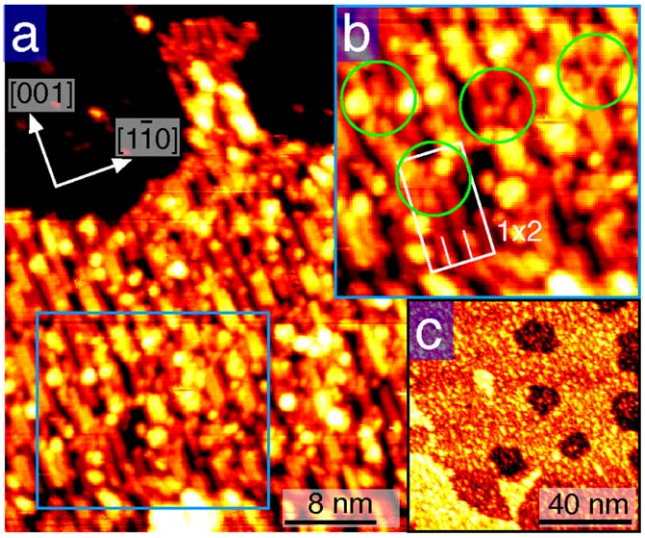

Figure 3. STM images of TiO_2(110) recorded from an inner beam region after exposure at 3 keV, 0.68 mA cm^{-2} for 10 min (e-exp 1). (a) 45 × 35 nm^2 image (1.52 V, 0.5 nA). (b) The zoom inset (blue) exhibits the presence of 1 × 2 areas (white) and crosslinked features (green). (c) 100 × 100 nm^2 image (1.5 V, 4.56 nA) that evidences the presence of typical terrace and step structure.

Electron gun irradiation of the 1 × 1 termination

TiO_2(110)1 × 1 surfaces were exposed to defocused 3 keV electron beams. STM images were then recorded in three areas which we denote as: (i) the inner beam region, with a 2 mm diameter around the beam centre (highest intensity); (ii) the outer beam region, near the outer edge of the beam, 3–5 mm diameter around the beam centre (lower intensity); and (iii) outside the beam. The positions were estimated by means of the e-beam illuminated spot profile on the phosphor coated sample plate, and with distances estimated with the aid of a video camera. The beam profile is assumed to be Gaussian with higher intensity in the centre of the beam, and the electron density reported is for the entire beam. Electron current densities of 0.6–0.7 mA cm^{-2} have been employed for durations of 10–40 min. All images reported here are recorded after an exposure of either 0.68 mA cm^{-2} for 10 min (e-exp 1) or 0.65 mA cm^{-2} for 40 min (e-exp 2). For the longer exposure times the observed effects are amplified, but are qualitatively comparable to the results for shorter exposures. It was observed that outside the beam area the surface remained clean and the defect density remained constant. However, the inner and outer regions of e-beam exposure displayed surface modifications, as discussed below.

Inner e-beam region modifications of TiO_2(110)

Figure 3 displays STM images recorded from the inner beam region after e-exp 1. The surface has lost 1 × 1 ordering and appears rough with features elongated in the [001] direction, ∼5 nm being the greatest length of individual features. Some of the features display 1 × n periodicity ($n \geqslant 2$), including 1 × 2 regions and crosslinking, as highlighted in figure 3(b). Although the surface has roughened, the (110) surface steps are maintained, as observed in larger scale STM images such as that of figure 3(c).

STM tip pulses of up to 10 V were performed on the inner beam region. Figure 4 shows the effect of such tip pulses. Large-scale reconstructions of the surface are induced with tip pulses above 5 V. Multiply-stepped 1 × 2 areas are observed with crosslinking, and regions of 1 × 1 reconstruction also form at the intersection of 1 × 2 steps. Figure 4(a) shows an image following a 7 V pulse. There is a ∼54 × 44 nm^2 oval reconstructed region elongated in the [001] direction. This oval shape is also exhibited in the overall step orientations in regions with multiple steps. As observed for pulses on the 1 × 1 surface, the size of the pulse-induced reconstruction is larger when the bias of the pulse is higher. Figure 4(b) shows an image taken after a 10 V pulse where a larger oval reconstructed area is observed that is ∼160 × 125 nm^2 in size. The 1 × 1, 1 × 2 and crosslink structures can be clearly observed in figure 4(c).

The e-beam exposed surface was also annealed to investigate the effect of heating on the transformation of the surface and to gain insight into the oxygen composition by observing the surface structures formed. The crystal was annealed to ∼850 K for 5 min. Typical STM images recorded from the inner beam region of e-exp 2 after this anneal are shown in figure 5. While the surface is still rough, the e-beam damaged surface has clearly reconstructed: small terraces have formed with 1 × 1 and dispersed 1 × 2 reconstructions. The 1 × 2 regions display crosslinking, whilst the 1 × 1 surface contains individual O_{vac} or OH_{br} point defects (figure 5(b)). Further annealing to normal preparation temperatures (∼1000 K) completely lifts any e-beam induced reconstruction and returns the surface to the 1 × 1 phase.

Outer e-beam region and flash anneal modifications of TiO_2(110)

Figure 6(a) shows a representative STM image from the outer beam region, where the beam intensity was lower. The surface is essentially 1 × 1, but modification in the form of well-resolved atomic scale surface 'cracks' is observed. The surface steps are maintained as shown in the insert of figure 6(a). The exact orientations of the 'nano-cracks' are in the principal crystallographic directions that terrace steps follow, i.e. [001], [1$\bar{1}$1] and [$\bar{1}$11]. Therefore, it is likely that the structures are atomically ordered. Figure 6(b) shows enlarged images of some of the various atomic scale structures observed on these surfaces, including 'zipper' type [001] oriented cracks (in the green box), [$\bar{1}$11] type single (in the purple box) and double (in the blue box) line cracks, and staggered cracks composed of both types. Although the surface displays 1 × 1-like order, with [001] direction rows, the contrast does not match that expected for normal imaging of as-prepared surfaces. In figure 6(b), dashed blue lines with 1 × 1 periodicity are placed on the image with one line exactly in the centre of the crack. These lines highlight the relative positions of the centre of the [001] crack and the features on the surface. It is apparent that the brighter features on the surface are in registry with the centre of the [001] crack. Therefore, if the

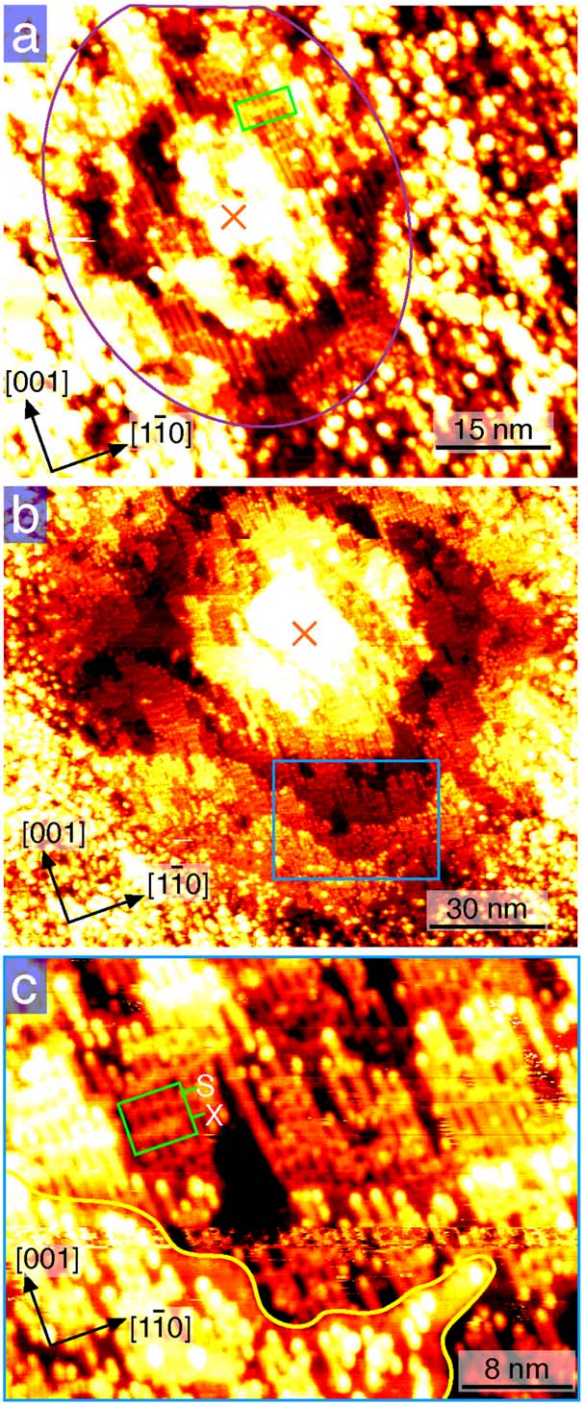

Figure 4. STM images of TiO_2(110) recorded after tip pulses on the inner beam region of the surface exposed to an e-beam at 3 keV, 0.65 mA cm^{-2} for 40 min (e-exp 2). (a) 73 × 60 nm^2 image following a 7 V tip pulse (V_{im} = 1.52 V, I_{im} = 0.3 nA, V_p = 7 V, t_p = 1 ms). The purple oval highlights the boundary of the pulse-induced reconstruction. (b) 150 × 120 nm^2 image following a 10 V pulse (V_{im} = 1.97 V, I_{im} = 0.3 nA, V_p = 7 V, t_p = 1 ms). The pulse profile is also oval, and contains four terraces separated by steps. (c) 41 × 32 nm^2 image (1.97 V, 0.3 nA), being a zoom into the area highlighted in (b) (blue box) displaying the 1 × 1 terraces and areas of 1 × 2, including single links (S) and crosslinks (X) (green box). The yellow line highlights the region of 1 × 1 terrace bound by a step edge. Orange crosses identify the lateral positions of tip pulses.

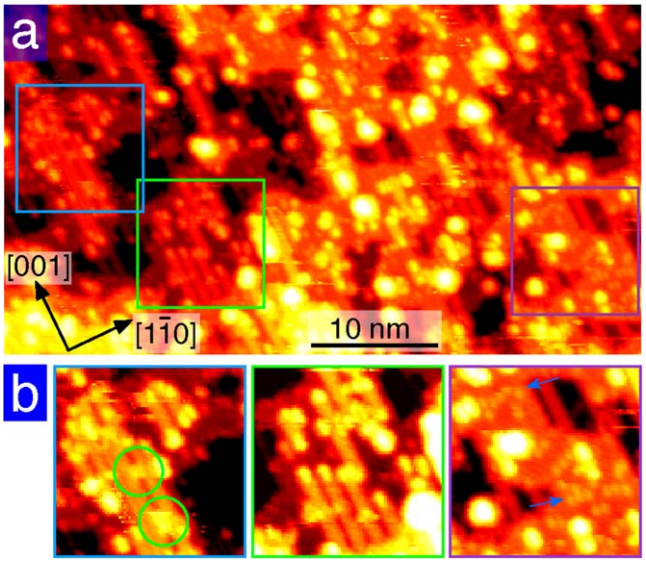

Figure 5. STM images recorded from the inner beam region of the e-beam exposed surface (3 keV, 0.65 mA cm^{-2}, 40 min, e-exp 2) after annealing the sample to ~850 K. (a) 49 × 35 nm^2 (1.83 V, 0.36 nA) The surface has reconstructed to small areas of 1 × 1 and 1 × 2 domains. (b) (10 nm)^2 enlarged areas from (a) show: (blue box) crosslinks (green circles) on the 1 × 2 reconstruction; (green box) 1 × 2 reconstruction; (purple box) individual point defects (i.e. O_{vac} or OH_{br}, blue arrows) on a 1 × 1 area.

bright features on the terraces are indeed OH_{br} defects, then the [001] cracks will be centred on the O_{br} rows of the surface. However, to elucidate the exact structures of the crack structures, more detailed information is needed.

Similar structures were prepared on clean 1 × 1 surfaces after preparation cycles of sputtering and annealing to ~1000 K followed by flash annealing the sample to ~570 K without further sputtering. The sample temperature was estimated by measuring the temperature of the sample plate in contact with the sample using an optical pyrometer. The reported flash temperature of 570 K is expected to be within ±100 K of the actual temperature of the sample surface. Figure 7 shows a surface prepared in such a way. Surface cracks like those observed in the outer e-beam region in figure 6 are seen. Figure 7(a) displays a high resolution image where surface defects and crack structures can be identified. The 'zipper' type [001] cracks are dominant, with a very low occurrence of the [$\bar{1}$11] type single and double line cracks. The large bright features on the terraces that are two O_{br} rows wide are the precursor structures to the growth of added row Ti_2O_3 structures. O_{vacs} are easily observed on this surface and can be seen to have a high concentration in comparison to previously reported O_{vac} densities. Normal sputter/anneal preparations give an O_{vac} concentration of 5%–10% with surfaces displaying morphology changes above 10% [29], whilst we have previously shown that an e-beamed surface with an O_{vac} concentration of 12% shows signs of pit formation [1]. On the current surface the O_{vacs} are observed in highly ordered regions, including c(4 × 2) (nominal O_{vac}

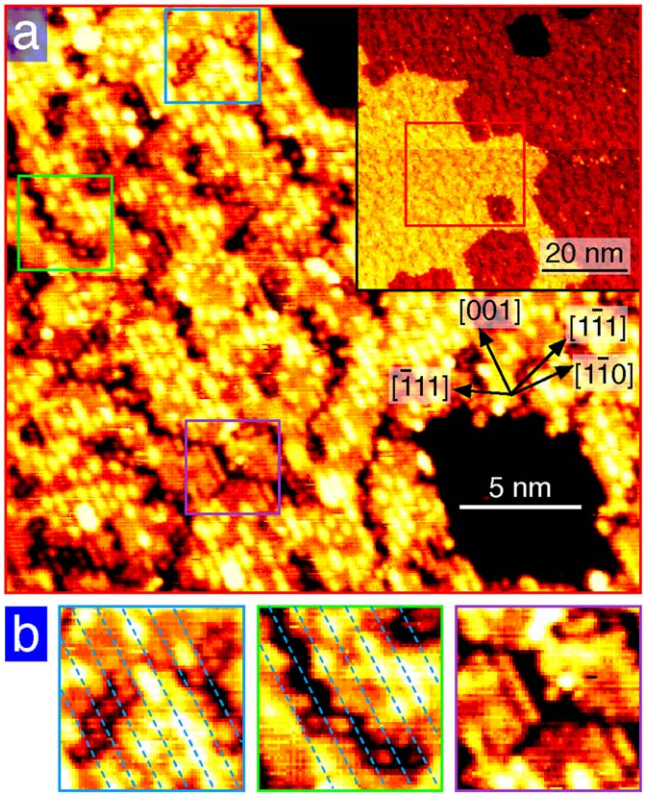

Figure 6. STM images recorded from an outer beam region after e-beam exposure at 3 keV, 0.68 mA cm^{-2} for 10 min (e-exp 1) (a) 26 × 24 nm^2 (1.5 V, 0.37 nA). The 1 × 1 surface is modified in the form of apparent 'nano-cracks'. The insert (65 nm)^2 shows the retention of typical step structures. The red box highlights the region shown in (a). (b) 8 × 8 nm^2 enlarged areas from (a) show: (blue box) a zig–zig type double line crack region; (green box) an [001] oriented zipper type crack which merges into a zig–zag region; (purple box) a region of single line cracks that highlights the three main crystallographic directions adopted by the cracks. The dashed blue lines with a 6.5 Å unit cell spacing indicate the position of the centre of the zipper crack with respect to bright features on the terrace.

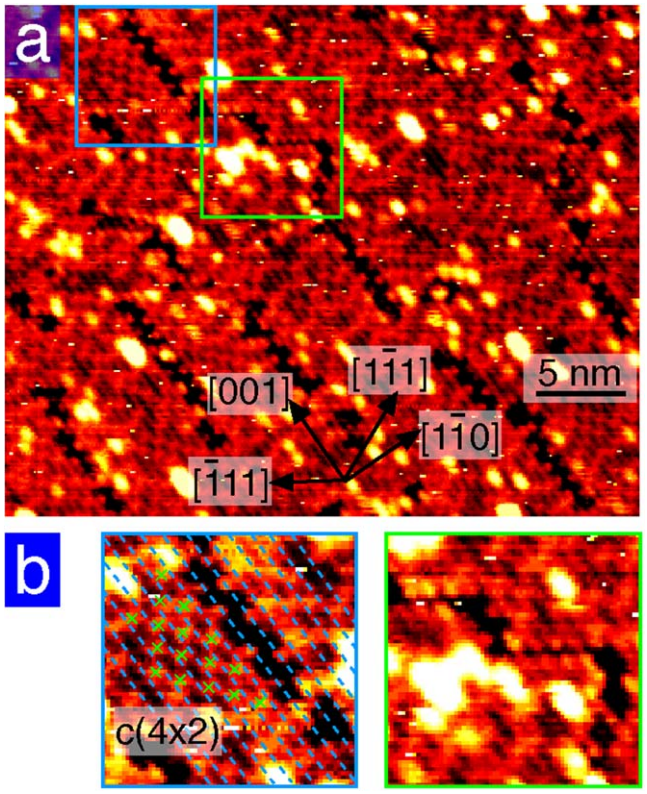

Figure 7. STM images recorded from a clean TiO_2(110)1 × 1 sample after several flash anneals to ~570 K. (a) 36 × 30 nm^2 (1.5 V, 0.5 nA). The surface has a high O_{vac} concentration and displays areas of ordered O_{vac} and nano-cracks, similar to those in figure 6. (b) 7 × 7 nm^2 enlarged areas from (a) display: (blue box) an area of c(4 × 2) O_{vacs} (green crosses), and a well resolved zipper type crack, with dashed blue lines (6.5 Å unit cell spacing) highlighting the position of the bright Ti_{5f} rows with respect to the crack; (green box) a region that highlights two of the three main crystallographic directions adopted by the cracks.

concentration of 25%) and with regular separation along the [001] rows directly adjacent to the zipper cracks. The bright features in the zipper cracks also have a regular separation of ~1.2 nm. The zoomed image of figure 7(b) shows the c(4 × 2) O_{vacs} and a zipper type crack structure (blue box). The blue dashed lines indicate the position of the bright Ti 5-fold rows with respect to the crack structure. It is clear that the bright features in the crack correspond to Ti atoms, and the crack is indeed centred on the O_{br} row, as identified on the e-beam prepared surface. The [$\bar{1}$11] type single crack is clearly distinguished in the expanded green box in figure 7(b).

Figure 8 displays a tip pulse at 10 V on the outer beam region. Tip pulses create a 1 × 2 reconstruction at the centre of the pulse as it does on the clean 1 × 1 surface. The pulse was performed near a step and the induced reconstruction is observed to incorporate both of the terraces. Additionally, it is observed that the 'cracked' surface around the pulse 'heals' to

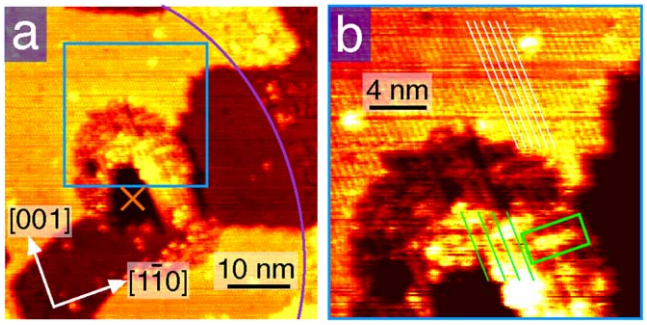

Figure 8. STM images recorded after a tip pulse on an outer beam region of the e-beam exposed surface at 3 keV, 0.68 mA cm^{-2} for 10 min (e-exp 1) (a) 50 × 50 nm^2 10 V pulse (V_{im} = 1.52 V, I_{im} = 0.5 nA, V_p = 10 V, t_p = 1 ms). The purple line indicates the boundary of the 'healed' 1 × 1 termination at ~70 × 50 nm^2 in size with an oval profile, elongated in the [001] direction. (b) 20 × 20 nm^2. An enlarged region of the tip pulse highlighting the 1 × 1 periodicity (white lines), the 1 × 2 reconstruction (green lines) and crosslinking (green box). The blue box in (a) indicates the area of (b). The orange cross indicates the position of the tip pulse.

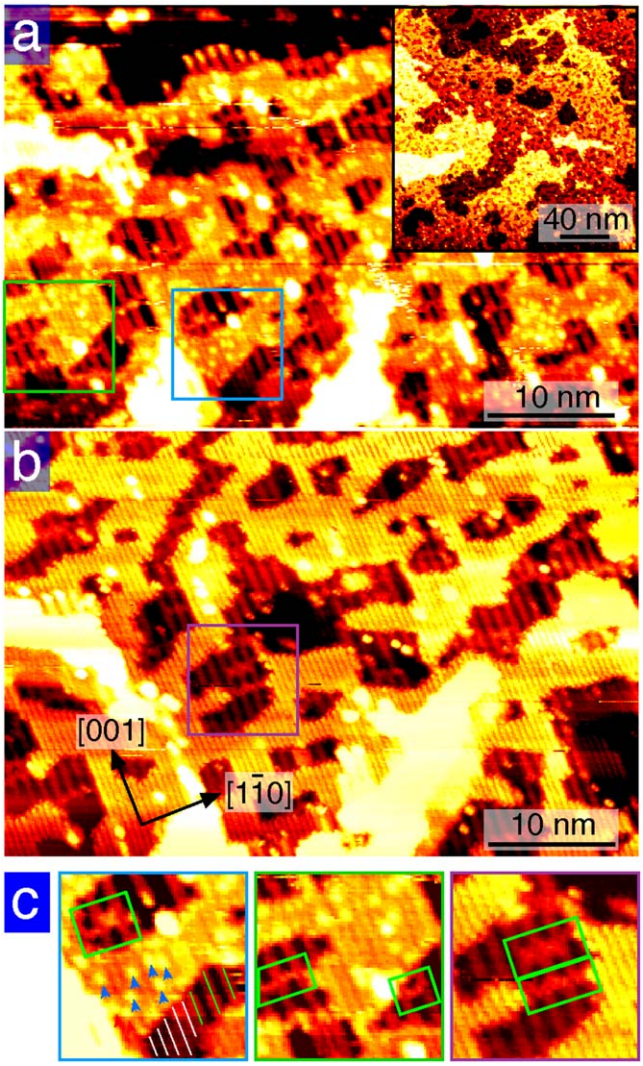

Figure 9. STM images recorded from an outer beam region of the e-beam exposed surface (3 keV, 0.65 mA cm^{-2} for 40 min, e-exp 2) after annealing the sample to ~850 K. (a) and (b) both 50 × 33 nm^2 (1.83 V, 0.36 nA) show a flat mixed 1 × 1/1 × 2 terminated surface. The insert in (a) 200 × 200 nm^2 shows a large scale image which displays the retention of typical step structures. (c) 8 × 8 nm^2. Enlarged areas from (a) and (b) including (blue box) individual point defects (i.e. O_{vac} or OH_{br}, blue arrows) on a 1 × 1 area, and a mixed 1 × 1/1 × 2 terrace (white and green lines respectively). 1 × 2 reconstructed regions with single links and crosslinks are highlighted with green boxes.

recover the 1 × 1 order of the clean surface. Beyond the healed region, the 'nano-cracks' remain unaltered. The profile of both the centre 1 × 2 reconstruction and the healed 1 × 1 region is oval, with elongation in the [001] direction. Figure 8(b) displays the 1 × 1 and 1 × 2 periodicity, as well as the crosslinking on the 1 × 2 region.

The outer beam region was also imaged after annealing the crystal to ~850 K for 5 min. The images shown in figure 5 and figure 9 were recorded on the same crystal after a single anneal. Typical STM images recorded from the outer beam region after this anneal are shown in figure 9. Large terraces with layered 1 × 1 and 1 × 2 reconstructions have formed, with the appearance that the 1 × 2 reconstruction is buried within the 1 × 1 terraces. Figures 9(a) and (b) display different imaging modes that highlight different aspects of the surface. Figure 9(a) is the 'normal' imaging mode, where individual O_{vac} or OH_{br} point defects can be imaged, and highlights the presence of these point defects on the 1 × 1 surface regions. Figure 9(b) is an imaging mode that highlights better the periodicity of the surface terraces with higher contrast. Figure 9(c) shows zoomed images that help to identify the point defects on the 1 × 1 surface (blue box) and single links and crosslinks on the 1 × 2 regions (green and purple boxes). Further annealing to normal preparation temperatures (~1000 K) also lifts the outer region e-beam induced reconstruction and returns the surface to the 1 × 1 phase.

We move on to discuss the tip induced effects observed on the clean TiO_2(110)1 × 1 surface. Then we discuss the insight that tip pulse induced reconstructions give into the oxygen content of the e-beam exposed surfaces. Finally, we discuss the detail of the surface modification in the outer e-beam irradiated surface, and its comparison with the structures prepared by heating the crystal.

Tip induced modifications on the rutile TiO_2(110) surface have been reported for various tunnelling and tip pulse conditions, and lead to a variety of differing structures. Previously we have reported the formation of 1 × 2 reconstructions on the TiO_2(110)1 × 1 surface, with domain sizes of around 6–8 nm at pulse settings of 5–10 V and tunnelling currents of 0.2–0.5 nA [1]. The latter are higher than those used in the present study (0.02 nA). We observed that the 1 × 1 to 1 × 2 reconstruction is also reversible to some extent by consecutive pulses in close proximity. This suggests a transfer of material on the surface during the tip pulse, as material is also added to the surface. Due to the large surface modification observed it was difficult to trace the movement of material precisely. At the lower tunnelling currents employed here, it is easier to identify the movement of material during the tip pulse. The central region of the tip pulse is crater-like, and added material appears around this crater. Therefore it is likely that material removed from the centre by the tip pulse is redeposited onto the surface around the crater, forming the oxygen deficient TiO_{2-x} structures, such as the 1 × 2 rows and rosette structures. The high resolution images enable us to conclude that the added features have a well-ordered atomic structure. The tip pulse also clearly affects a wider area around the central region, as seen by the removal of OH_{br}.

The oval shape that we observe in tip pulse features is likely to arise from the anisotropic conductivity of electrons deposited in the pulse, which is higher in the [001] direction as compared to the [1$\bar{1}$0] direction, as reported in [27].

The mechanism for removal of oxygen is likely to be an Auger process, which is common for metal oxides. The low energy secondary electrons (<200 eV) produced by the high energy electron beam (3 keV) generate Auger transitions in the Ti-O system that causes removal of O by multiple electron loss. The neutral or positively charged O can only escape at the surface [2, 30].

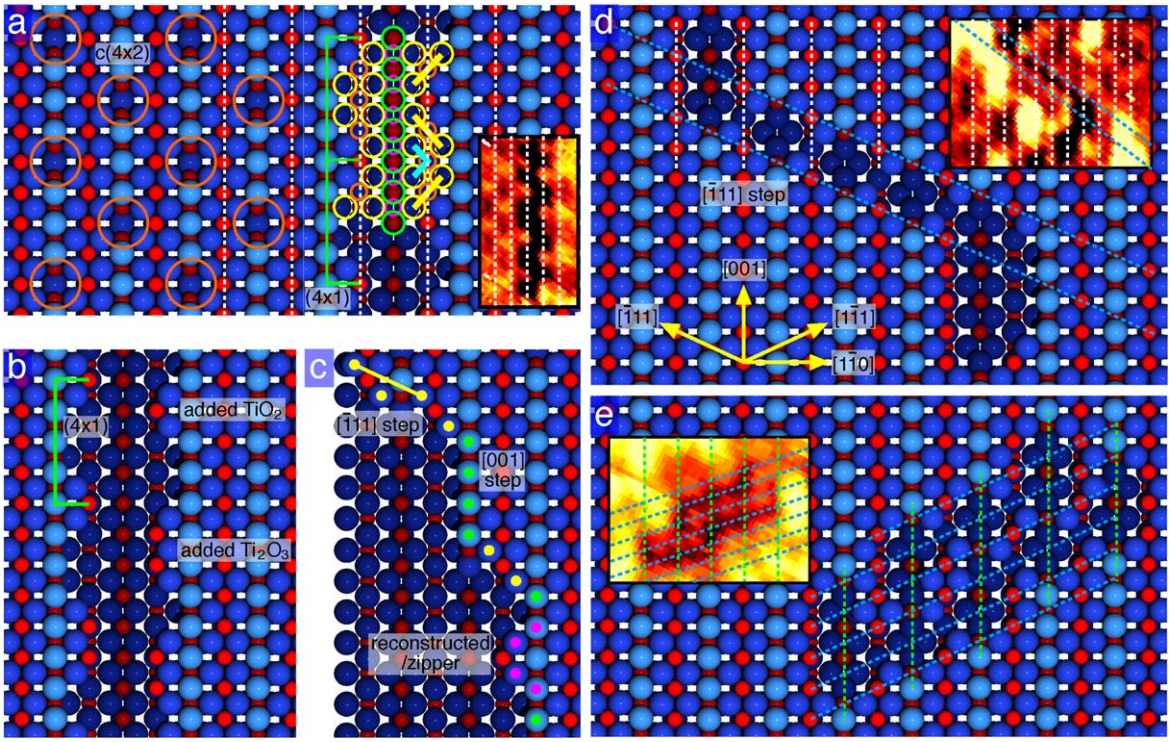

Figure 10. Ball model of the proposed surface crack structures of figures 6 and 7. Blue and red balls correspond to O and Ti atoms respectively, with lighter colours indicating atoms protruding further from the surface. (a) The c(4 × 2) O_{vac} arrangement is highlighted with orange circles. The insert is from figure 7(b). Dashed white lines highlight the bright Ti rows. The [001] oriented crack is modelled. Circles show missing units which are all TiO_2 stoichiometry (yellow–orange–yellow and green–purple–green). The thick yellow and blue lines highlight an example of the TiO_2 units removed in the surface plane (yellow–orange–yellow). The green line highlights the nominally 4 × 1 zipper type reconstructed features attributed to added single TiO_2 units at the [001] step edge [6]. (b) Again the green line indicates a 4 × 1 zipper type feature. Also displayed are non-4 × 1 proposed structures for larger features in the crack attributed to added Ti_2O_3 units at the [001] step edge. (c) Step edge structures as proposed in [6] are shown with dots in yellow [$\bar{1}$11] oriented and green [001] oriented steps. The purple dots highlight the position of the added TiO_2 unit that gives rise to the reconstructed [6] or zipper-type structure. (d) Proposed single line-crack structures. Dashed white lines highlight the bright Ti rows. The dashed blue lines highlight the [$\bar{1}$11] direction, comparable with the step edge structure in (c). The insert is from figure 7(b). (e) Proposed double line-crack structures. The insert is from figure 6(b) with dashed green lines highlighting the O_{br} rows. Dashed blue lines highlight the [1$\bar{1}$1] direction. The structures are essentially a combination of the normal step structures in the [$\bar{1}$11], [1$\bar{1}$1] and [001] crystallographic directions.

All of the e-beam induced effects that we observe are lifted by annealing the crystal to normal preparation temperatures. This is in contrast to the formation of 1 × 2 surfaces via bulk reduction, where annealing to lower temperatures does not regenerate the 1 × 1 surface. Instead, reoxidation of the 1 × 2 surface is needed to regenerate the 1 × 1 surface [20, 28, 31, 32]. Hence, the e-beam induced modification of the surface affects only the near surface, and is reversible due to the ability of TiO_2 surfaces to heal themselves by exchange of oxygen from the bulk to the oxygen deficient surface (or via migration of reduced interstitial Ti species). This is in line with our previous results on e-beam exposure using lower (75–300 eV) energy electrons to generate near-surface modifications.

Further evidence that the e-beam effects are only at the near surface come from the effect of tip pulsing on the heavily oxygen deficient inner-beam region. The regions of 1 × n periodicity ($n \geqslant 2$) seen after the e-beam exposure and the resulting mixed 1 × 1/1 × 2 surface after the 850 K anneal are indicative of high oxygen deficiency. When the tip pulses are performed on this e-beamed surface the large-scale reconstructions observed are surprising. They are high-energy, highly reduced surface terminations with well defined atomic-ordering, including multiple steps and 1 × 2 structures with crosslinking. This suggests that the oxygen deficient surface, although highly energetically unfavourable and very rough, retains substantial structural ordering within the near surface.

The modified surface structures in the outer-beam region and the anneal at ~570 K are similar in nature. They can be explained by means of structural models based on the autocompensated step edge structures proposed in [6]. Figure 10 shows a surface model with proposed nano-crack structural features and corresponding STM images for comparison. In [6], [001] step edge structures are either terminated in O_{br} rows (dark termination) or with nominally 4 × 1 reconstructed bright features, which are attributed to an 'added' TiO_2 unit where the Ti is 3-fold coordinated (Ti-3f). For autocompensation to occur, the same number of Ti-O bonds and O-Ti bonds must be broken, forming stable surface terminations. In figure 10(a) a proposed TiO_2-unit removal is shown as a way to represent the local charge neutrality and stoichiometry compensation, allowing structural identification of removed units in the cracks. In our images a zipper-type

crack is formed from two [001]-oriented steps separated by one $[1\bar{1}0]$ unit cell, with staggered Ti-3f on each step. Sometimes larger (Ti_xO_{x+1}, $x > 1$) units are observed in the crack, and periodicity not equal to 4×1 is present (figure 10(b)). In the case of $[\bar{1}11]$-type single line cracks (figure 10(d)), the cracks consist of $[\bar{1}11]$-type steps separated by one [001] unit cell and change from $[\bar{1}11]$- to [001]-oriented cracks with a mixture of [001] edges terminating in the dark O_{br} steps and bright features attributed to a Ti-3f termination. Finally, for $[\bar{1}11]$-type double line cracks (figure 10(e)), the crack structure is similar to that of single line cracks, with the exception of the bright features between the dark cracks corresponding to Ti-3f or −4f as they would be at normal step edges.

It is instructive to compare features observed in the images of an e-beamed surface with those from a surface flash-annealed in UHV that are shown in figures 6 and 7, respectively. From these images we can see that single- and double-line $[\bar{1}11]$-type cracks are dominant on the e-beamed surface, whilst double-line cracks are absent on the annealed surface. Moreover, [001]-oriented cracks are dominant on the annealed surface, with longer cracks than that observed on the e-beamed surface; both surfaces are likely to have a high level of ordering of O_{vac}. This gives insight into the relative formation energies of the features: in the annealed surface the oxygen deficient defective structures are likely to be subject to diffusion effects to generate the longer [001] cracks and highly ordered c(4 × 2) O_{vac}. Also, once the cracks start to form the thermal energy from annealing will overcome the low energy barrier to crack-propagation of the stable phase step edge-like structures. In contrast, the e-beamed surface preparation involves a limited input of thermal energy. The structures are proposed to be formed via direct electronic excitation leading to bond breaking, therefore spatially constraining the formation of features to where they occur, and leading to the generation of higher energy structures such as the formation of Ti-3f in the double-line crack.

Conclusions

E-beam stimulated processes have been used to modify the surface structure of TiO_2(110) surfaces. It has been possible to generate localised reconstruction to what are usually high temperature structures produced after reduction of the crystal in the bulk. We have also observed novel atomically ordered nano-crack structures produced with two different preparations. These processes are reversible, as annealing to preparation temperatures (∼1000–1100 K) reforms the 1×1 surface. Our results demonstrate that the oxygen composition and structure of the TiO_2(110) surface can be modified in a controllable and reversible fashion using STM and electron beam irradiation. This provides the tools with which to create patterned structures and modified areas for subsequent nanofabrication and altered reactivity, enabling selective surface functionalisation.

Acknowledgments

This work was supported by the European Research Council Advanced Grant ENERGYSURF (GT), European Cooperation in Science and Technology Action CM1104, EPSRC (UK) through contract GR/S23506/01, and the Alexander von Humboldt Stiftung (Germany). GT is also supported by the Royal Society through a Royal Society Wolfson Research Merit Award.

ORCID iDs

Chi L Pang https://orcid.org/0000-0002-5222-9734
Qiao Chen https://orcid.org/0000-0001-5424-4818
Geoff Thornton https://orcid.org/0000-0002-1616-5606

References

[1] Pang C L *et al* 2006 *Nanotechnology* **17** 5397–405
[2] Dulub O, Batzill M, Solovev S, Loginova E, Alchagirov A, Madey T E and Diebold U 2007 *Science* **317** 1052–6
[3] Hallam T, Butcher M J, Goh K E J, Ruess F J and Simmons M Y 2007 *J. Appl. Phys.* **102** 034308
[4] Vollnhals F, Woolcot T, Walz M-M, Seiler S, Steinrück H-P, Thornton G and Marbach H 2013 *J. Phys. Chem.* C **117** 17674–9
[5] Pang C L, Lindsay R and Thornton G 2013 *Chem. Rev.* **113** 3887–948
[6] Diebold U, Lehman J, Mahmoud T, Kuhn M, Leonardelli G, Hebenstreit W, Schmid M and Varga P 1998 *Surf. Sci.* **411** 137–53
[7] Pang C L, Lindsay R and Thornton G 2008 *Chem. Soc. Rev.* **37** 2328–53
[8] Guo Q, Yin F and Palmer R E 2005 *Small* **1** 76–9
[9] Yin F, Palmer R E and Guo Q 2006 *Surf. Sci.* **600** 1504–9
[10] Schofield S R, Curson N J, Simmons M Y, Rueß F J, Hallam T, Oberbeck L and Clark R G 2003 *Phys. Rev. Lett.* **91** 136104
[11] Mayne A J, Riedel D, Comtet G and Dujardin G 2006 *Prog. Surf. Sci.* **81** 1–51
[12] Tanner R E, Castell M R and Briggs G A D 1998 *Surf. Sci.* **412–413** 672–81
[13] Klusek Z, Busiakiewicz A, Datta P K, Schmidt R, Kozlowski W, Kowalczyk P, Dabrowski P and Olejniczak W 2007 *Surf. Sci.* **601** 1513–20
[14] Berko A and Krivan E 1997 *J. Vac. Sci. Technol.* B **15** 25–31
[15] Onishi H and Iwasawa Y 1994 *Langmuir* **10** 4414–6
[16] Bikondoa O, Pang C L, Ithnin R, Muryn C A, Onishi H and Thornton G 2006 *Nat. Mater.* **5** 189–92
[17] Suzuki S, Fukui K-I, Onishi H and Iwasawa Y 2000 *Phys. Rev. Lett.* **84** 2156–9
[18] Mentes T O, Locatelli A, Aballe L, Pavlovska A, Bauer E, Pabisiak T and Kiejna A 2007 *Phys. Rev.* B **76** 155413
[19] Yim C M, Pang C L and Thornton G 2010 *Phys. Rev. Lett.* **104** 036806
[20] Bennett R A, Stone P, Price N J and Bowker M 1999 *Phys. Rev. Lett.* **82** 3831–4
[21] Takakusagi S, Fukui K-I, Nariyuki F and Iwasawa Y 2003 *Surf. Sci.* **523** L41–6
[22] Pang C L, Haycock S A, Raza H, Murray P W, Thornton G, Gulseren O, James R and Bullett D W 1998 *Phys. Rev.* B **58** 1586
[23] Onishi H and Iwasawa Y 1996 *Phys. Rev. Lett.* **76** 791–4

[24] Diebold U, Anderson J F, Ng K-O and Vanderbilt D 1996 *Phys. Rev. Lett.* **77** 1322–5
[25] Bowker M 2006 *Curr. Opin. Solid State Mater. Sci.* **10** 153–62
[26] Batzill M, Katsiev K, Gaspar D J and Diebold U 2002 *Phys. Rev.* B **66** 235401
[27] Byl O and Yates J T 2006 *J. Phys. Chem.* B **110** 22966–7
[28] Li M, Hebenstreit W, Gross L, Diebold U, Henderson M A, Jennison D R, Schultz P A and Sears M P 1999 *Surf. Sci.* **437** 173–90
[29] Wendt S *et al* 2005 *Surf. Sci.* **598** 226–45
[30] Knotek M L and Feibelman P J 1979 *Surf. Sci.* **90** 78–90
[31] Henderson M A 1999 *Surf. Sci.* **419** 174–87
[32] Stone P, Bennett R A and Bowker M 1999 *New J. Phys.* **1** 8